IEEE Photonics Journal
An IEEE Photonics Society Publication

Terahertz Reconfigurable Metasurface for Dynamic Non-Diffractive Orbital Angular Momentum Beams using Vanadium Dioxide

Volume 12, Number 3, June 2020

Ling Wang, *Student Member, IEEE*
Yang Yang, *Senior Member, IEEE*
Shufang Li, *Senior Member, IEEE*
Li Deng, *Member, IEEE*
Weijun Hong, *Member, IEEE*
Chen Zhang, *Student Member, IEEE*
Jianfeng Zhu, *Student Member, IEEE*
David McGloin

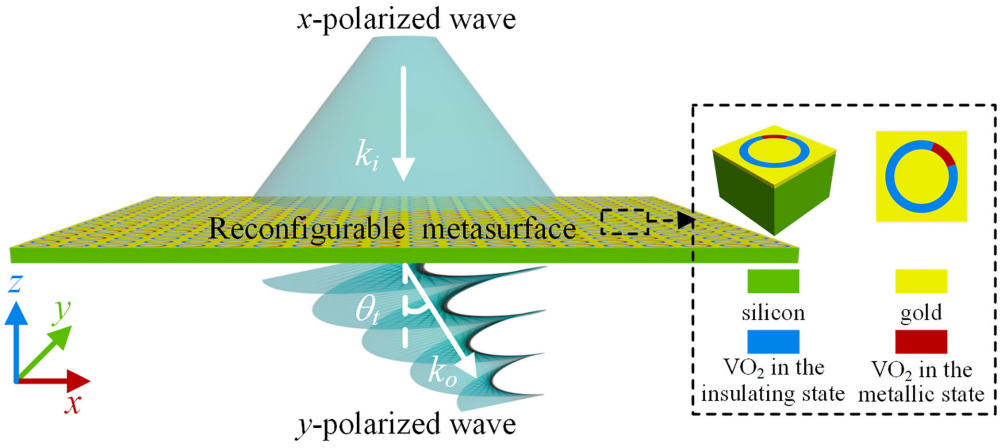

DOI: 10.1109/JPHOT.2020.3000779

Terahertz Reconfigurable Metasurface for Dynamic Non-Diffractive Orbital Angular Momentum Beams using Vanadium Dioxide

Ling Wang,[1,2,3] ***Student Member, IEEE*****,**
Yang Yang,[3] ***Senior Member, IEEE*****,**
Shufang Li,[1,2] ***Senior Member, IEEE*****, Li Deng,**[1,2] ***Member, IEEE*****,**
Weijun Hong,[1,2] ***Member, IEEE*****,**
Chen Zhang,[1,2] ***Student Member, IEEE*****,**
Jianfeng Zhu,[1,2,3] ***Student Member, IEEE*****, and David McGloin**[3]

[1]Beijing Key Laboratory of Network System Architecture and Convergence, Beijing University of Posts and Telecommunications, Beijing 100876, China
[2]Beijing Laboratory of Advanced Information Network, Beijing University of Posts and Telecommunications, Beijing 100876, China
[3]Tech Lab, School of Electrical and Data Engineering, University of Technology Sydney, Botany, NSW 2019, Australia

DOI:10.1109/JPHOT.2020.3000779

Manuscript received March 18, 2020; revised May 30, 2020; accepted June 4, 2020. Date of publication June 9, 2020; date of current version June 19, 2020. This work was supported in part by the Natural Science Foundation of Beijing under Grant 4202047, in part by the Beijing Nova Program under Grant Z181100006218039, and in part by the 111 Project (B17007). Corresponding authors: Shufang Li; Li Deng (e-mail: lisf@bupt.edu.cn; dengl@bupt.edu.cn).

Abstract: Orbital angular momentum (OAM) generation based on metasurfaces has attracted tremendous interest due to its potential in capacity enhancement of high-speed wireless communication systems. Reconfigurability is one of the key desired characteristics for the design of future metasurfaces. In this paper, a metasurface taking advantage of vanadium dioxide (VO_2) is proposed. The proposed design can generate a non-diffractive OAM beam and achieve the multiple reconfigurability of the topological charge, beam radius, beam deflection angle. The operation frequency can be adjusted by controlling the state of VO_2 at terahertz (THz) region. Simulation results demonstrate that the designed metasurface can generate a non-diffractive OAM beam with tunable topological charge and beam radius, propagating along $\pm x$ or $\pm y$ directions with the controllable deflection angle between 6.74° and 44.77°, ranging from 0.69 THz to 0.79 THz.

Index Terms: Terahertz (THz), reconfigurable metasurface, vanadium dioxide (VO_2), orbital angular momentum (OAM), topological charge (TC), non-diffractive beam, deflection angle.

1. Introduction

Electromagnetic (EM) waves have been demonstrated to carry angular momentum (AM), encompassing spin angular momentum (SAM) and orbital angular momentum (OAM) [1]–[3]. While SAM is associated with the circular polarization state of the wave and so it has a limited number of states, OAM manifests in the corkscrew-shaped phase in front of such beams. Therefore, the topological charge (denoted *l*) of an OAM beam is theoretically unlimited and mutually orthogonal to each

other. Recently, due to these properties, OAM has attracted tremendous interest in its ability to offer capacity enhancement of high-speed wireless communications [4], [5].

There are various ways to generate OAM beams, such as forked gratings [6], spiral phase plates (SPPs) [7], q plates [8], spiral reflectors [9], antenna arrays [10], cylindrical mode converters [11] and computer-generated holograms [12]. However, most of these technologies require high-precision processes and large components. Also, they work only within a narrow bandwidth, which significantly increases the system complexity and severely restricts practical applications. To tackle these challenges, recent advancement in metasurfaces offers a new horizon for OAM generation. As the two-dimensional (2D) version of metamaterials [13], metasurfaces [14] can effectively engineer the phase, polarization and amplitude of the EM waves via spatially variant abrupt phase changes. Metasurfaces, therefore, have versatile functionality, ultra-thin features, and ease-of-integration, and are ideally suited for OAM generation.

Previous research has mainly focused on producing OAM beams based on metasurfaces without tunable metaparticles. The majority of these metasurfaces are aimed at producing an OAM beam with a particular *l* [15], [16]; realizing multichannel superpositions of OAM states with various *l* values [17], [18]; or generating OAM beams with different topological charges at different wavelengths [19], [20], input beam intensities [21] and polarization states [22]. However, in general, these metasurfaces are not tunable or reconfigurable, which inherently limits their practical impact. In the optical regime, such control can be achieved straightforwardly using devices such as spatial light modulators [23], but such technology is not readily available in the microwave or THz bands. As such, in recent years, significant effort has been made to develop reconfigurable metasurfaces by employing tunable metaparticles, such as vanadium dioxide (VO_2) [24], indium tin oxide [25], graphene [26], liquid crystal [27] germanium antimony telluride (GST) [28], InSb/In0.8Al0.2Sb heterojunctions [29], micro-electromechanical systems (MEMS) [30], varactor diodes [31], and PIN diodes [32].

Although these methods have been successfully applied to implement metasurfaces, they have never been used to realize reconfigurable OAM beams in the terahertz (THz) range. The existing reconfigurable structures have only produced OAM beams with tunable *l* values propagating with a particular deflection angle at a single fixed frequency or a narrow band in the microwave range [33]–[35]. In addition, these OAM beams expand along the propagation direction, which limits power received at the receiver side in communication applications. Therefore, generating an OAM beam with multiple reconfigurability of the topological charge, beam radius, deflection angle and operating frequency simultaneously based the metasurface using tunable metapraticles, has become an emerging research area that requires dealing with formidable challenges, especially in THz applications, where the conventional microwave manipulation techniques are found to be impractical. Compared with other tunable metaparticles used at THz region, VO_2 exhibits an insulator-to-metal transition at around 67 degrees driven by temperature. The corresponding electrical conductivity increases by approximately five orders of magnitude in the THz region, providing a larger dynamic range using a phase transition. Thus, it is a very promising material for active control of electromagnetic properties for THz metasurface reconfigurability.

In this paper, a reconfigurable metasurface using VO_2 is proposed for the generation of a reconfigurable non-diffractive THz OAM beam. We present simulation results to demonstrate the reconfigurability. The proposed metasurface holds great potential for the capacity enhancement of high-speed wireless communication systems. This study can be used for the realization of software-defined wideband reconfigurable metasurfaces for THz applications.

2. Theory

VO_2 exhibits an insulator-to-metal transition driven by temperature [36], intense light [37] or charge flow [38]. Among these technologies, the temperature inspired approach is found to be more practical. As the temperature increases, the lattice structure of VO_2 is changed from monoclinic to tetragonal, resulting in an increased electrical conductivity by several orders of magnitude during

the insulator-to-metal transition at around 67 degrees. Generally, there are two ways to describe the complex dielectric properties of VO_2 in the THz region. The first method is based on the Bruggeman effective-medium theory (EMT) [39]. The relative permittivity of VO_2 is typically written as

$$\varepsilon_{VO_2}(V) = \frac{\varepsilon_i(2-3V) + \varepsilon_m(3V-1) + \sqrt{[\varepsilon_i(2-3V) + \varepsilon_m(3V-1)]^2 + 8\varepsilon_i\varepsilon_m}}{4} \tag{1}$$

where ε_i and ε_m are the relative permittivity of the insulating and metallic VO_2 films, respectively, and V is the volume fraction of the metallic regions.

The varied permittivity of VO_2 can also be described by the Drude model [40], as follows

$$\varepsilon_{VO_2}(\omega) = \varepsilon_\infty - \frac{\omega_p^2(\sigma_{VO_2})}{\omega^2 + i\gamma\omega} \tag{2}$$

where $\varepsilon_\infty = 12$ is dielectric permittivity at the infinite frequency, $\gamma = 5.75 \times 10^{13}$ rad/s is the collision frequency, $\omega_p(\sigma_{VO_2})$ is the plasma frequency depending on the conductivityσ_{VO_2}which is approximately described as

$$\omega_p^2(\sigma_{VO_2}) = \frac{\sigma_{VO_2}}{\sigma_0}\omega_p^2(\sigma_0) \tag{3}$$

where $\sigma_0 = 3 \times 10^3\ \Omega^{-1}\text{cm}^{-1}$ and $\omega_p(\sigma_0) = 1.4 \times 10^{15}$ rad/s.

We note that the temperature-dependent conductivityσ_{VO_2}can also be used to quantify the dynamic insulator-to-metal transition of VO_2. The relative permittivity of VO_2 films in the insulating state is nine and in the metallic state is described by Drude model, while the conductivity in the fully insulating and metallic state is smaller than 2×10^2 S/m and higher than 2×10^5 S/m [41]–[43].

To generate an OAM vortex beam with topological charge l based on the metasurface, the spatially varying phase distributions of the metasurface must satisfy the following equation [44]

$$\varphi_l(x, y) = l \cdot \arctan\frac{y}{x},\ l = \pm1, \pm2, \ldots \tag{4}$$

where (x, y) is the arbitrary position on the metasurface plane. In addition, when $l = 0$, the beam is a plane wave.

Generally, there are two methods to control the radius of the beam. A direct method is to focus the beam at a specific position, and another method is to generate a non-diffractive beam, such as a Bessel beam [45], [46]. The latter is more preferable than the former, because the non-diffractive beam can propagate along the path with more concentrated energy distribution compared with the converging beam. According to the designing principle of the non-diffractive beam generated through the axicon lens [47], the phase distribution of the metasurface can be described as

$$\varphi_B(x, y) = \frac{2\pi}{\lambda}\sqrt{x^2 + y^2}\sin\beta \tag{5}$$

where λ is the working wavelength, (x, y) is the arbitrary position on the metasurface plane, and β is the base angle of the axicon.

According to the generalized Snell's law of refraction [48], when the EM wave incident to the interface vertically along the z-axis ($\theta_i = 0$) and $n_i = n_t = 1$, the angle of refraction can be expressed as follows

$$\begin{aligned}\theta_t(x) &= \arcsin\left(\frac{\lambda}{2\pi}\cdot\frac{d\varphi}{dx}\right)\\ \theta_t(y) &= \arcsin\left(\frac{\lambda}{2\pi}\cdot\frac{d\varphi}{dy}\right)\end{aligned} \tag{6}$$

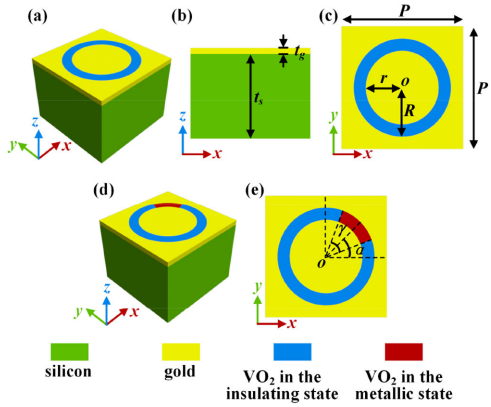

Fig. 1. (a) The unit cell of the metasurface consists of a ring slot filled with VO_2 on a gold sheet and a silicon substrate. (b), (c) The side view and top view of the unit cell. Geometric parameters are the following: $P = 100$ μm, $t_s = 70$ μm, $t_g = 0.2$ μm, $R = 40$ μm, and $r = 30$ μm. (d), (e) Different phase responses can be simply achieved by switching the state of a part of the VO_2 loop between insulator and metal without physically changing the structure. The azimuth angle α is the angle between the symmetric axis of the VO_2 in the metallic state and the x-axis. γ is the angle of the metallic VO_2 arc.

where λ is the working wavelength. To realize beam steering, the phase distribution of the tilt wavefront for the four different directions along $\pm x$ and $\pm y$ directions is described as follows

$$\begin{aligned} \varphi_{tx}(x) &= \pm\frac{2\pi}{D}\cdot x \\ \varphi_{ty}(y) &= \pm\frac{2\pi}{D}\cdot y \end{aligned} \tag{7}$$

where D is the super-unit-cell period along the phase gradient direction. Obviously, according to Equations (6) and (7), the angle of refraction θ_t is a function of λ and D.

Therefore, in order to generate a non-diffractive OAM beam with desired l value and the base angle β, propagating along the $\pm x$ or $\pm y$ directions with the required deflection angle θt at the working frequency f, we superposed the OAM vortex phase distributions, the Bessel beam phase distributions, and the tilt phase distributions as follows

$$\begin{aligned} \varphi_{l,Beseel,tilt}(x,y) &= \varphi_l + \varphi_B + \varphi_{tx} \\ &= l\cdot\arctan\frac{y}{x} + \frac{2\pi}{\lambda}\sqrt{x^2+y^2}\sin\beta \pm \frac{2\pi}{D}\cdot x \\ \varphi_{l,Beseel,tilt}(x,y) &= \varphi_l + \varphi_B + \varphi_{ty} \\ &= l\cdot\arctan\frac{y}{x} + \frac{2\pi}{\lambda}\sqrt{x^2+y^2}\sin\beta \pm \frac{2\pi}{D}\cdot y \end{aligned} \tag{8}$$

3. The Design of Unit Cell and Metasurface

3.1 Unit Cell

The unit cell of the proposed reconfigurable metasurface is sketched in Fig. 1(a), 1(b) and 1(c), which consists of a ring slot filled with VO_2 on a gold sheet and a silicon substrate. The period of the unit cell is $P = 100$ μm. The silicon substrate is assumed to have the relative permittivity of 11.9 with a thickness of $t_s = 70$ μm. The gold is 0.2 μm thick. $R = 40$ μm and $r = 30$ μm are the outer and inner radii of the ring slot. Different phase responses can be achieved by switching the states of a part of the ring-shaped VO_2 between insulator and metal, without physically changing the structure, as shown in Fig. 1(d) and 1(e). According to the theory proposed by N. F. Yu *et al.* [48], the V-antennas support "symmetric" and "antisymmetric" modes and arbitrary phases of the

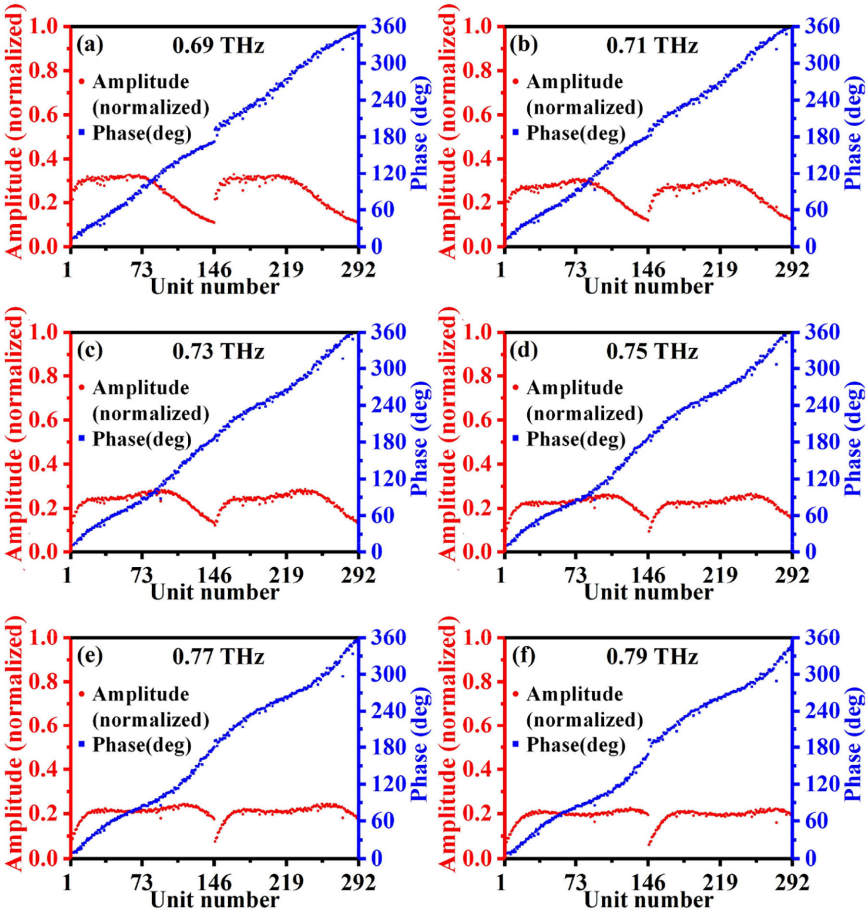

Fig. 2. The amplitude and phase of cross-polarized transmitted wave radiation from 292 different unit cells numbered from 1 to 146 and 147 to 292 corresponding to $\alpha = 45°$ and $-45°$, respectively, while γ is linearly stepping from 5° to 150° with a step width of 1°. (a) 0.69 THz. (b) 0.71 THz. (c) 0.73 THz. (d) 0.75 THz. (e) 0.77 THz. (f) 0.79 THz.

scattered wave can be obtained by adjusting the geometric parameters of the antenna. Since there are both two points for the C-shaped and V-shaped antenna, they hold similar properties. Thus, C-shaped slot antennas also can be used to control the scattered wave. When a linearly-polarized EM wave impinges on the unit cell, both symmetric and antisymmetric modes can be excited, and a cross-polarized field is then scattered by these two modes. The amplitude and phase of the re-emitted field can then be modulated by adjusting the geometrical parameters of the C-shaped slot antennas, which can be changed by switching the state of a part of the VO_2 loop. α is the angle between the symmetric axis of the VO_2 in the metallic state and the *x*-axis. γ is the angle of the metallic VO_2 arc.

In the simulation, periodic boundary conditions are set in the *x*- and *y*- directions and are open in the *z*-direction under the condition of free space. A Floquet excitation port is applied in the unit cell, making use of ANSYS HFSS software. The unit cell is normally illuminated by an *x*-polarized incident wave. In addition, the relative permittivity of VO_2 films in the insulating state is set as 9 and in the metallic state is described by Drude model, while the conductivity of VO_2 in the fully insulating and metallic state is set to 2×10^2 S/m and 2×10^5 S/m, respectively. 292 different units are numbered from 1 to 146 and 147 to 292, corresponding to $\alpha = 45°$ and $-45°$, respectively, while γ linearly steps from 5° to 150° in 1° steps. Based on the simulation, we find that the phase of the transmitted cross-polarized THz wave modulated from 0 to 2π and generated from 292 different

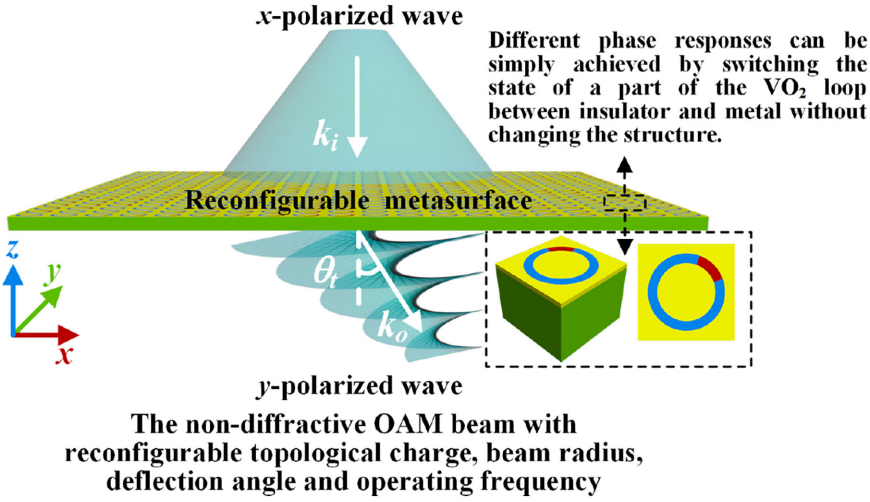

Fig. 3. The illustration of the reconfigurable metasurface and expected electromagnetic functionalities. When a linearly-polarized EM wave impinges on the metasurface, both symmetric and antisymmetric modes can be excited, and a cross-polarized field is then scattered by these two modes. Different phase responses can be simply achieved by switching the state of a part of the VO_2 loop between insulator and metal without physically changing the structure. Therefore, a non-diffractive OAM beam with reconfigurable topological charge, beam radius, deflection angle, and operating frequency can be generated.

units, can cover 2π at frequencies ranging from 0.69 THz to 0.79 THz. Here, we just take six single frequency points, which are 0.69 THz, 0.71 THz, 0.73 THz, 0.75 THz, 0.77 THz, and 0.79 THz, for example. Fig. 2 presents the amplitudes and phase of cross-polarized transmission wave radiation from 292 different units at these six frequency points.

3.2 Metasurface

Fig. 3 shows an illustration of the reconfigurable metasurface and expected electromagnetic functionalities.

The proposed reconfigurable metasurface is composed of 20 $\times$ 20 unit cells of the type depicted in Fig. 1(a). By independently controlling the states of VO_2 hybridized into the slot shown in Fig. 1(d), such a metasurface can manipulate the cross-polarized transmission phase, as shown in Fig. 2. Thus, this metasurface expects to achieve the desired reconfigurability of the deflection angle and generate a non-diffractive OAM beam with defined l and base angle β, propagating along $\pm x$ or $\pm y$ directions with the desired deflection angle θ_t.

The process to obtain the required reconfigurable metasurface is as follows: firstly, divide the continuous phase from 0 to 2π into M equal parts. Then, select M units corresponding to M parts, while maintaining the cross-polarized phase difference of transmitted waves $\Delta\varphi = \frac{2\pi}{M}$ between two adjacent units. After that, the phase values of the metasurface should be wrapped within the range from 0 to 2π and quantized into M values. Finally, corresponding units at different positions of the metasurface are determined. M can be any integer between 6 and 36 based on the phase characteristics of these 292 units. Suitable units can be selected according to Fig. 2. In addition, based on Equations (6) and (7), the deflection angle θ_t of the beam is a function of D and $D = M \times P$. Therefore, θ_t varies with M and can be calculated as

$$\theta_t = \arcsin\left(\pm\frac{\lambda}{D}\right) = \arcsin\left(\pm\frac{\lambda}{M \cdot P}\right) \tag{9}$$

In this paper, we take $l = -2$ and 4, $\beta = 50°$, 30° and 20°, $M = 36$, 18 and 6 and $f = 0.71$ THz ($\lambda = 422.54$ μm), for example, to demonstrate the reconfigurability our device and for verification of

TABLE 1
The Number of Selected Three Groups of Unit Cells and Corresponding Calculated $\Delta\varphi$ and $|\theta_t|$ with M = 36, 18 and 6 Respectively at 0.71 THz

M	The number of selected units	$\Delta\varphi$ (°)	$\lvert\theta_t\rvert$ (°)
36	2, 8, 16, 28, 36, 47, 57, 68, 78, 80, 89, 96, 100, 106, 117, 123, 132, 145, 147, 153, 160, 166, 182, 191, 200, 213, 222, 228, 236, 243, 246, 256, 264, 269, 282, 291	10	6.74
18	2, 15, 36, 57, 78, 89, 102, 114, 133, 150, 164, 185, 200, 221, 236, 246, 264, 279	20	13.58
6	2, 57, 102, 150, 200, 246	60	44.77

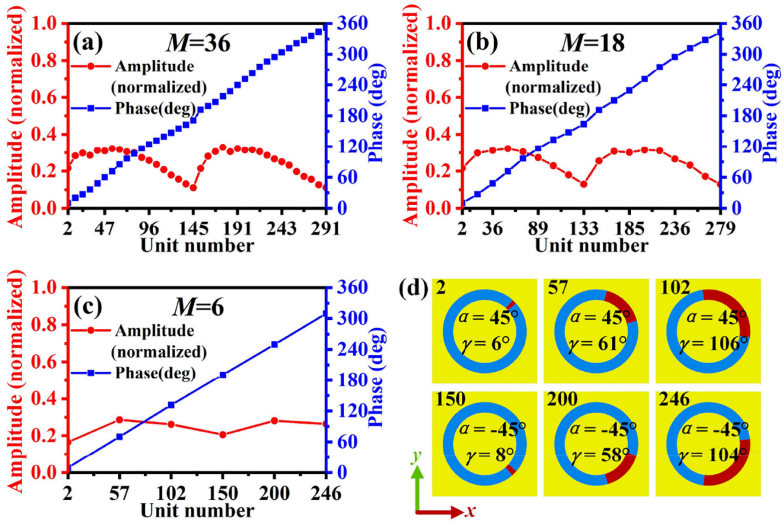

Fig. 4. (a), (b), and (c) Simulated amplitudes and phases of the cross-polarized transmitted wave radiation from three groups of units with $M = 36$, 18 and 6 respectively. (d) The top view of one group of units with $M = 6$. Units numbered 2, 57 and 102 have $\alpha = 45°$ and $\gamma = 6°$, 61° and 106°, respectively. Units numbered 150, 200 and 246 have $\alpha = -45°$ and $\gamma = 8°$, 58° and 104°, respectively.

non-diffractive OAM beam generation. The required l and β propagates along $\pm x$ or $\pm y$ directions with the desired θ_t at the working frequency f.

The number of three illustrative groups of units and corresponding $\Delta\varphi$ and $|\theta_t|$ are shown in Table 1. We note that since the minimum $\Delta\varphi$ is 10° this is a lower limit. As long as units of a selected group satisfy the chosen $\Delta\varphi$ other units may be selected. Fig. 4(a), 4(b), and 4(c) show simulated amplitudes and phases of the cross-polarized transmitted wave radiation from these three groups of units. The schematic of one group of units is also depicted in Fig. 4(d).

4. Generation of OAM Beam

4.1 Generating an OAM Beam With a Reconfigurable l at the Working Frequency

First, to verify this metasurface can generate an OAM beam with reconfigurable l at the working frequency, simulation of the EM characteristics of the reconfigurable metasurface that produces an OAM beam with $l = -2$ or $+4$ and $M = 36$, 18 and 6 respectively is conducted according to the Equation (4). An x-polarized terahertz plane wave usually illuminates the metasurface along the negative direction of the z-axis. d is the distance from the bottom of the metasurface. The schematics of the metasurface and simulated amplitude and phase distributions of the transmitted cross-polarized wave at the yoz plane and a plane parallel to the xoy plane with $d = 3\lambda$ are shown in Fig. 5. According to the simulation results, OAM beams with $l = -2$ and $+4$ can be generated by this reconfigurable metasurface with $M = 36$, 18, and 6 respectively at 0.71 THz. This verifies that a VO_2 based metasurface offers the desired reconfigurability.

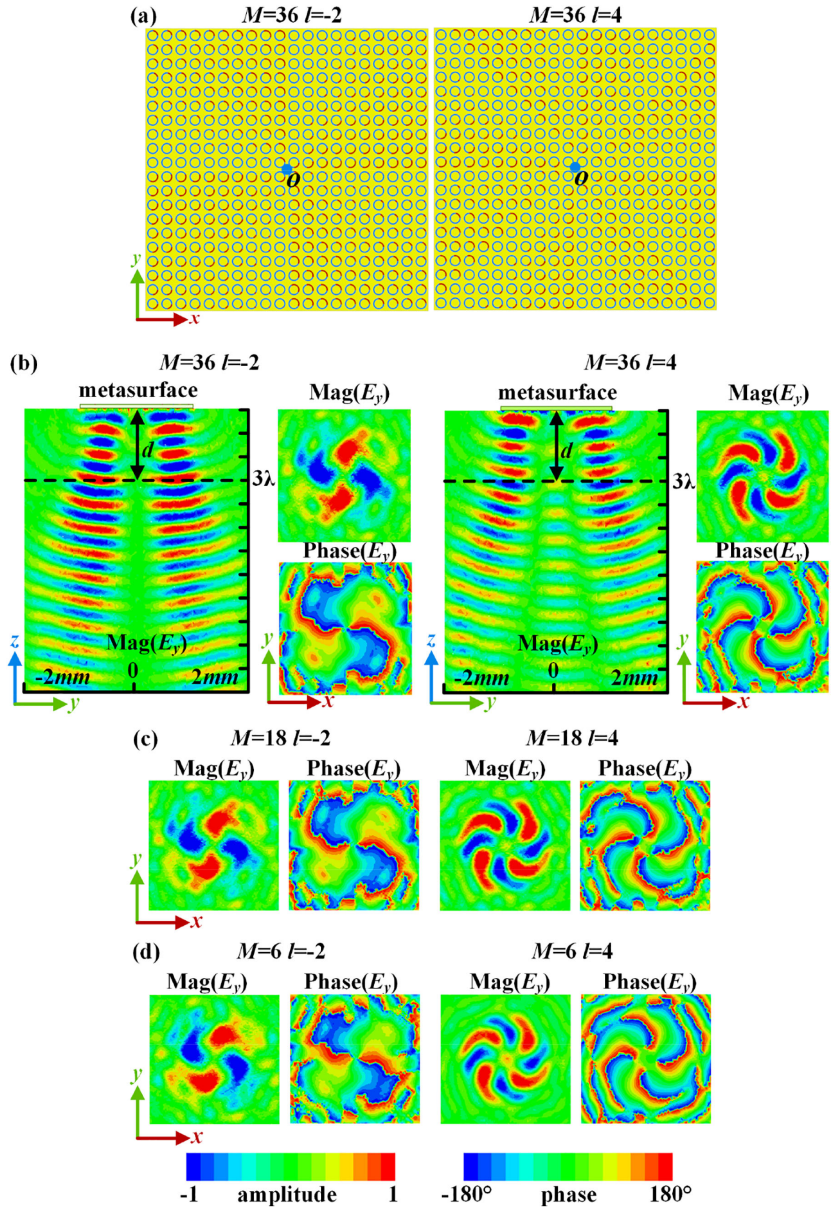

Fig. 5. The schematics of the metasurface and simulated amplitude and phase distributions of the transmitted cross-polarized wave at the *yoz* plane and a plane parallel to the *xoy* plane with $d = 3\lambda$. (a) The schematics of the metasurface with $M = 36$, $l = -2$, and 4. Amplitude and phase distributions with (b) $M = 36$, $l = -2$, and 4. (c) $M = 18$, $l = -2$, and 4. (d) $M = 6$, $l = -2$, and $l = 4$.

4.2 Generating a Non-Diffractive OAM Beam With a Reconfigurable Beam Radius

Secondly, to verify this metasurface can generate a reconfigurable non-diffractive OAM beam, simulation of the EM characteristics of the reconfigurable metasurface that generates a non-diffractive OAM beam with $l = +4$, $M = 36$ and $\beta = 50°$, 30° and 20° respectively is conducted by superposing Equations (4) and (5). The simulated amplitude and phase distributions of the transmitted cross-polarized wave at the *yoz* plane and planes parallel to the *xoy* plane with *d* linearly stepping from 1.5λ to 6.5λ with a step width of 1λ, are shown in Fig. 6(b), (c) and (d). As a contrast, the simulated results of this metasurface generating a pure OAM beam with $l = +4$ and $M = 36$ in corresponding *xoy* planes are also depicted in Fig. 6(a). According to the simulation results,

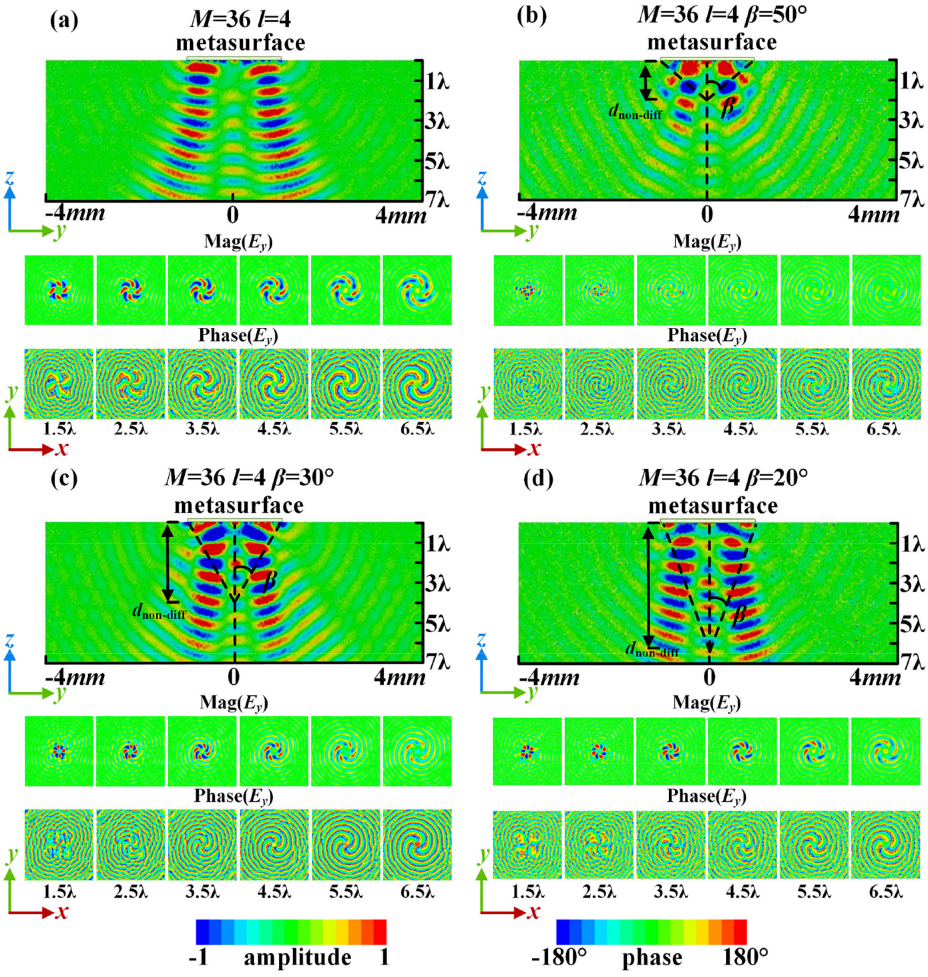

Fig. 6. Comparison of a pure OAM beam and non-diffractive OAM beams with reconfigurable beam radius are generated by the metasurface. The simulated amplitude and phase distributions of the transmitted cross-polarized wave at the *yoz* plane and planes parallel to the *xoy* plane with *d* linearly stepping from 1.5λ to 6.5λ with a step width of 1λ. (a) A pure OAM beam with $M = 36$, $l = 4$. A non-diffractive OAM beam with $M = 36$, $l = 4$ and (b) $\beta = 50°$. (c) $\beta = 30°$. (d) $\beta = 20°$.

it can be observed clearly that non-diffractive OAM beams with $l = +4$, $M = 36$ and $\beta = 50°$, 30° and 20° can be generated by this reconfigurable metasurface at 0.71 THz, and the corresponding non-diffractive distance $d_{\text{non-diff}}$ equals 0.84 mm, 1.73 mm and 2.75 mm respectively.

4.3 Generating an OAM Beam With a Reconfigurable Deflection Angle

We also verify that the metasurface can be engineered to deflect the beam at the desired angle. We investigate this using an OAM beam with $l = +4$ propagating along the $+y$ or $-y$ direction with $|\theta_t| = 6.74°$, 13.58°, and 44.77° modeled by superimposing Equation (4) and (7). The simulated amplitude and phase distributions of the transmitted cross-polarized wave at the *yoz* plane and planes with $\theta = 0°$ and $|\theta_t|$ are shown in Fig. 7(b), 7(d) and 7(f). As a contrast, the simulated results of this metasurface generating an OAM beam with $l = +4$ and $\theta_t = 0°$ in corresponding planes are also depicted in Fig. 7(a), 7(c) and 7(e). In Fig. 7(a), 7(c) and 7(e), because of $|\theta_t| = 0°$, we can see that there is no deflection at the *yoz* plane, and the amplitude and phase distributions of the OAM vortex beam at the plane with $\theta = 0°$ is better than the plane with $\theta = 6.47°$, 13.58° and 44.77° respectively.

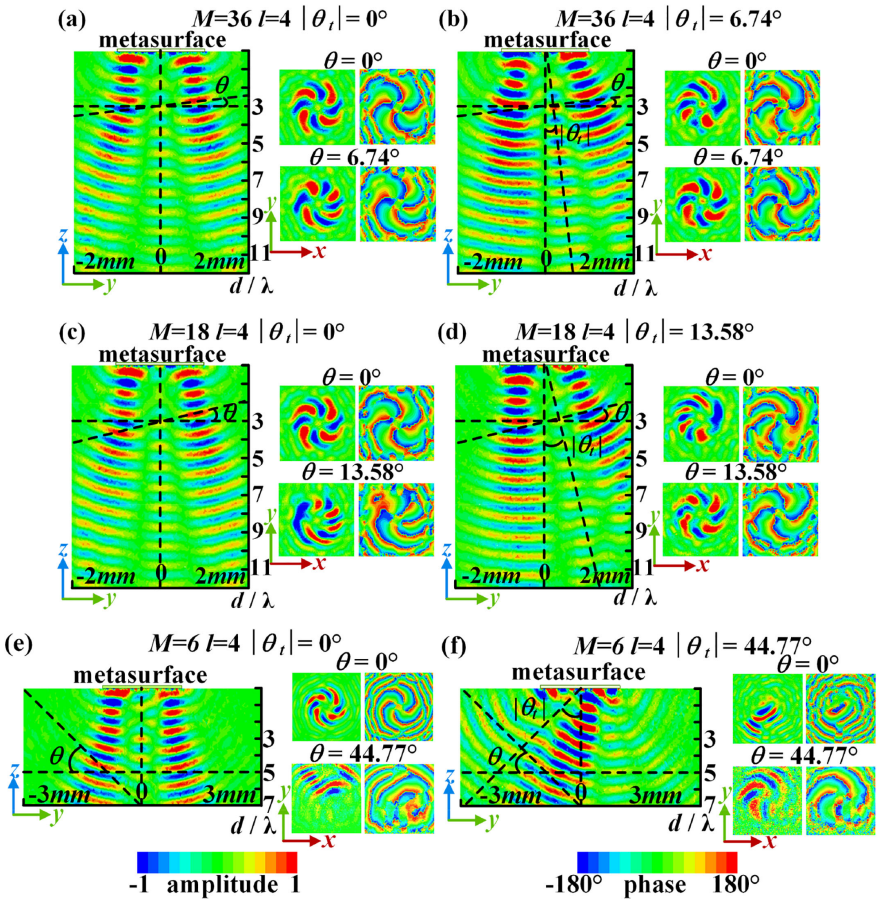

Fig. 7. OAM beams with reconfigurable refraction angle are generated by the metasurface. The simulated amplitude and phase distributions of the transmitted cross-polarized wave at the *yoz* plane and planes with $\theta = 0°$ and $|\theta_t|$. (a) $M = 36$, $l = 4$ and $|\theta_t| = 0°$. (b) $M = 36$, $l = 4$ and $|\theta_t| = 6.47°$. (c) $M = 18$, $l = 4$ and $|\theta_t| = 0°$. (d) $M = 18$, $l = 4$ and $|\theta_t| = 13.58°$. (e) $M = 6$, $l = 4$ and $|\theta_t| = 0°$. (f) $M = 6$, $l = 4$ and $|\theta_t| = 44.77°$.

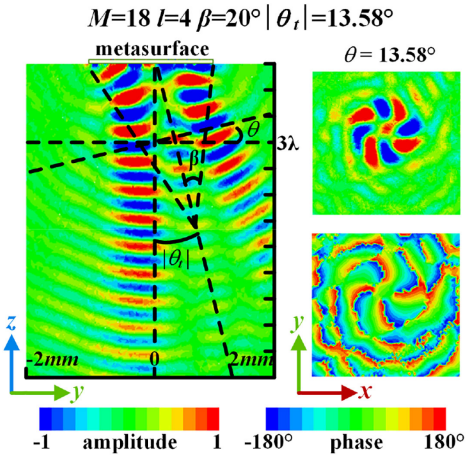

Fig. 8. A non-diffractive OAM beam with $l = +4$ and $\beta = 20°$ propagating along the $+y$ direction with $\theta_t = 13.58°$ is generated by the metasurface. Simulated amplitude and phase distributions of the transmitted cross-polarized wave at the *yoz* plane and planes with $\theta = 0°$ and $|\theta_t|$.

Similarly, in Fig. 7(b), 7(d) and 7(f), because of $|\theta_t| = 6.47°$, 13.58° and 44.77° respectively, the beam is deflected, and the amplitude and phase distributions of the OAM vortex beam at the plane with $\theta = 6.47°$, 13.58° and 44.77°, respectively, is better than the plane with $\theta = 0°$.

4.4 Generating a Non-Diffractive OAM Beam With a Specified l, Beam Radius and Deflection Angle

Finally, we combine the results from 4.1, 4.2 and 4.3 to generate a fully reconfigurable beam. We model a non-diffractive OAM beam with $l = +4$ and $\beta = 20°$ propagating along the $+y$ direction with $\theta_t = 13.58^\circ$ making use of Equation (8). Simulated amplitude and phase distributions of the transmitted cross-polarized wave at the *yoz* plane and planes with $\theta = 0°$ and $|\theta_t|$ are shown in Fig. 8.

5. Conclusion

In conclusion, we have proposed and demonstrated that a reconfigurable metasurface based on VO_2 is a viable component for the generation of fully tunable THz beams ranging from 0.69 THz to 0.79 THz in terms of their OAM content, coupled with non-diffractive and beam steering capabilities. This is achieved without the need to alter the physical metasurface, but via a tuning mechanism that depends on the VO_2 state via its thermal properties. The proposed metasurface holds great potential for capacity enhancement of high-speed wireless communication systems. This study can be extended to software-defined wideband reconfigurable metasurface at terahertz frequencies.

Future works will focus on experimentally verifying the performance of the designed metasurface. The photolithography and micro-fabrication process can be used to fabricate the proposed metasurface. The challenge is how to locally control the desired heating. We suggest that this is achievable, making use of a resistive heater or for finer control via exposure to a continuous wave (CW) laser, making use of a beam steering element to target the desired heating points. We note that all-optical control of VO_2 devices is also emerging [49], and our work feeds into a developing field that will further fuse optical and THz control for next-generation communication systems.

References

[1] L. Allen, S. M. Barnett, and M. J. Padgett, *Optical Angular Momentum*. Boca Raton, FL, USA: CRC Press, 2016.
[2] J. P. Torres and L. Torner, *Twisted Photons: Applications of Light With Orbital Angular Momentum*. Hoboken, NJ, USA: Wiley, 2011.
[3] L. Allen, M. W. Beijersbergen, R. J. C. Spreeuw, and J. P. Woerdman, "Orbital angular momentum of light and the transformation of Laguerre-Gaussian laser modes," *Physical Rev. A*, vol. 45, no. 11, pp. 8185–8189, 1992.
[4] A. E. Willner *et al.*, "Optical communications using orbital angular momentum beams," *Adv. Opt. Photon.*, vol. 7, no. 1, pp. 66–106, 2015.
[5] Y. Yan *et al.*, "High-capacity millimetre-wave communications with orbital angular momentum multiplexing," *Nature Commun.*, vol. 5, 2014, Art. no. 4876.
[6] V. Y. Bazhenov, M. V. Vasnetsov, and M. S. Soskin, "Laser-beams with screw dislocations in their wave-fronts," *Jetp Lett.*, vol. 52, no. 8, pp. 429–431, 1990.
[7] M. Beijersbergen, R. Coerwinkel, M. Kristensen, and J. Woerdman, "Helical-wavefront laser beams produced with a spiral phase plate," *Opt. Commun.*, vol. 112, no. 5-6, pp. 321–327, 1994.
[8] L. Marrucci, C. Manzo, and D. Paparo, "Optical spin-to-orbital angular momentum conversion in inhomogeneous anisotropic media," *Physical Rev. Lett.*, vol. 96, no. 16, 2006, Art. no. 163905.
[9] F. Tamburini *et al.*, "Encoding many channels in the same frequency through radio vorticity: First experimental test," *New J. Phys.*, vol. 14, no. 3, 2012, Art. no. 033001.
[10] D. Comite, G. Valerio, M. Albani, A. Galli, M. Casaletti, and M. Ettorre, "Exciting vorticity through higher order bessel beams with a radial-line slot-array antenna," *IEEE Trans. Antennas Propag.*, vol. 65, no. 4, pp. 2123–2128, 2017.
[11] M. J. Padgett and L. Allen, "Orbital angular momentum exchange in cylindrical-lens mode converters," *J. Opt. B: Quantum Semiclassical Opt.*, vol. 4, no. 2, pp. S17–S19, 2002.
[12] N. R. Heckenberg, R. McDuff, C. P. Smith, and A. G. White, "Generation of optical phase singularities by computer-generated holograms," *Opt. Lett.*, vol. 17, no. 3, pp. 221–223, 1992.
[13] R. A. Shelby, D. R. Smith, and S. Schultz, "Experimental verification of a negative index of refraction," *Science*, vol. 292, no. 5514, pp. 77–79, 2001.
[14] D. M. Lin, P. Y. Fan, E. Hasman, and M. L. Brongersma, "Dielectric gradient metasurface optical elements," *Science*, vol. 345, no. 6194, pp. 298–302, 2014.

[15] R. C. Devlin, A. Ambrosio, N. A. Rubin, J. P. B. Mueller, and F. Capasso, "Arbitrary spin-to–orbital angular momentum conversion of light," *Science*, vol. 358, no. 6365, pp. 896–900, 2017.
[16] Y. Z. Ran, J. G. Liang, T. Cai, and H. P. Li, "High-performance broadband vortex beam generator using reflective Pancharatnam–Berry metasurface," *Opt. Commun.*, vol. 427, pp. 101–106, 2018.
[17] Y. C. Zhang, W. W. Liu, J. Gao, and X. D. Yang, "Generating focused 3D perfect vortex beams by plasmonic metasurfaces," *Adv. Opt. Mater.*, vol. 6, no. 4, 2018, Art. no. 1701228.
[18] H. Zhao, B. G. Quan, X. K. Wang, C. Z. Gu, J. J. Li, and Y. Zhang, "Demonstration of orbital angular momentum multiplexing and demultiplexing based on a metasurface in the terahertz band," *ACS Photon.*, vol. 5, no. 5, pp. 1726–1732, May 2018.
[19] M. Yannai *et al.*, "Spectrally interleaved topologies using geometric phase metasurfaces," *Opt. Express*, vol. 26, no. 23, pp. 31031–31038, 2018.
[20] Z. Li *et al.*, "Tripling the capacity of optical vortices by nonlinear metasurface," *Laser Photon. Rev.*, vol. 12, no. 11, 2018, Art. no. 1800164.
[21] Y. Xu *et al.*, "Nonlinear metasurface for structured light with tunable orbital angular momentum," *Appl. Sci.*, vol. 9, no. 5, 2019, Art. no. 958.
[22] Y. Chen, X. D. Yang, and J. Gao, "Spin-selective second-harmonic vortex beam generation with babinet-inverted plasmonic metasurfaces," *Adv. Opt. Mater.*, vol. 6, no. 19, 2018, Art. no. 1800646.
[23] S. Q. Li, X. Xu, R. M. Veetil, V. Valuckas, R. Paniagua-Domínguez, and A. I. Kuznetsov, "Phase-only transmissive spatial light modulator based on tunable dielectric metasurface," *Science*, vol. 364, no. 6445, pp. 1087–1090, 2019.
[24] M. K. Liu *et al.*, "Terahertz-field-induced insulator-to-metal transition in vanadium dioxide metamaterial," *Nature*, vol. 487, no. 7407, pp. 345–348, 2012.
[25] A. Forouzmand and H. Mosallaei, "Tunable two dimensional optical beam steering with reconfigurable indium tin oxide plasmonic reflectarray metasurface," *J. Opt.*, vol. 18, no. 12, 2016, Art. no. 125003.
[26] L. Deng, Y. Y. Zhang, J. F. Zhu, and C. Zhang, "Wide-band circularly polarized reflectarray using graphene-based pancharatnam-berry phase unit-cells for terahertz communication," *Materials*, vol. 11, no. 6, 2018, Art. no. 956.
[27] M. Decker *et al.*, "Electro-optical switching by liquid-crystal controlled metasurfaces," *Opt. Express*, vol. 21, no. 7, pp. 8879–8885, 2013.
[28] Q. Wang *et al.*, "Optically reconfigurable metasurfaces and photonic devices based on phase change materials," *Nature Photon.*, vol. 10, no. 1, 2016, Art. no. 60-U75.
[29] P. P. Iyer, M. Pendharkar, and J. A. Schuller, "Electrically reconfigurable metasurfaces using heterojunction resonators," *Adv. Opt. Mater.*, vol. 4, no. 10, pp. 1582–1588, 2016.
[30] E. Arbabi, S. M. Kamali, Y. Horie, M. Faraji-Dana, and A. Faraon, "MEMS-tunable dielectric metasurface lens," *Nature Commun.*, vol. 9, no. 1, 2018, Art. no. 812.
[31] C. Huang *et al.*, "Reconfigurable metasurface cloak for dynamical electromagnetic illusions," *ACS Photon.*, vol. 5, no. 5, pp. 1718–1725, 2018.
[32] C. Huang, C. L. Zhang, J. N. Yang, B. Sun, B. Zhao, and X. G. Luo, "Reconfigurable metasurface for multifunctional control of electromagnetic waves," *Adv. Opt. Mater.*, vol. 5, no. 22, 2017, Art. no. 1700485.
[33] J. Q. Han, L. Li, H. Yi, and Y. Shi, "1-bit digital orbital angular momentum vortex beam generator based on a coding reflective metasurface," *Opt. Mater. Express*, vol. 8, no. 11, pp. 3470–3478, 2018.
[34] C. C. Li, L. S. Wu, and W. Y. Yin, "A dual-polarized and reconfigurable reflectarray for generation of vortex radio waves," *AIP Adv.*, vol. 8, no. 5, 2018, Art. no. 055331.
[35] J. Han, L. Li, H. Yi, and W. Xue, "Versatile orbital angular momentum vortex beam generator based on reconfigurable reflective metasurface," *Japanese J. Appl. Phys.*, vol. 57, no. 12, 2018, Art. no. 120303.
[36] A. M. N. F. Zylbersztejn and N. F. Mott, "Metal-insulator transition in vanadium dioxide," *Physical Rev. B*, vol. 11, no. 11, 1975, Art. no. 4383.
[37] M. F. Becker, A. B. Buckman, R. M. Walser, T. Lépine, P. Georges, and A. Brun, "Femtosecond laser excitation of the semiconductor-metal phase transition in VO_2," *Appl. Phys. Lett.*, vol. 65, no. 12, pp. 1507–1509, 1994.
[38] H. T. Kim *et al.*, "Mechanism and observation of Mott transition in VO_2-based two-and three-terminal devices," *New J. Phys.*, vol. 6, no. 1, 2004, Art. no. 52.
[39] P. U. Jepsen *et al.*, "Metal-insulator phase transition in a VO_2 thin film observed with terahertz spectroscopy," *Physical Rev. B*, vol. 74, no. 20, 2006, Art. no. 205103.
[40] Q. Chu, Z. Song, and Q. H. Liu, "Omnidirectional tunable terahertz analog of electromagnetically induced transparency realized by isotropic vanadium dioxide metasurfaces," *Appl. Phys. Exp.*, vol. 11, no. 8, 2018, Art. no. 082203.
[41] P. Mandal, A. Speck, C. Ko, and S. Ramanathan, "Terahertz spectroscopy studies on epitaxial vanadium dioxide thin films across the metal-insulator transition," *Opt. Lett.*, vol. 36, no. 10, pp. 1927–1929, 2011.
[42] T. T. Lv *et al.*, "Hybrid metamaterial switching for manipulating chirality based on VO_2 phase transition," *Scientific Rep.*, vol. 6, 2016, Art. no. 23186.
[43] F. Ding, S. Zhong, and S. I. Bozhevolnyi, "Vanadium dioxide integrated metasurfaces with switchable functionalities at terahertz frequencies," *Adv. Opt. Mater.*, vol. 6, no. 9, 2018, Art. no. 1701204.
[44] E. Karimi, S. A. Schulz, I. De Leon, H. Qassim, J. Upham, and R. W. Boyd, "Generating optical orbital angular momentum at visible wavelengths using a plasmonic metasurface," *Light: Sci. Appl.*, vol. 3, no. 5, 2014, Paper e167.
[45] D. McGloin and K. Dholakia, "Bessel Beams: Diffraction in a new light," *Contemporary Phys.*, vol. 46, pp. 15–28, 2005.
[46] Y. H. Guo, L. S. Yan, W. Pan, and B. Luo, "Generation and manipulation of orbital angular momentum by all-dielectric metasurfaces," *Plasmonics*, vol. 11, no. 1, pp. 337–344, 2015.
[47] Z. Jaroszewicz and J. Morales, "Lens axicons: Systems composed of a diverging aberrated lens and a perfect converging lens," *J. Opt. Soc. America A*, vol. 15, no. 9, pp. 2383–2390, 1998.
[48] N. Yu *et al.*, "Light propagation with phase discontinuities: Generalized laws of reflection and refraction," *Science*, vol. 334, no. 6054, pp. 333–337, 2011.
[49] S. C. Chen *et al.*, "All optically driven memory device for terahertz waves," *Opt. Lett.*, vol. 45, no. 1, pp. 236–239, 2020.